Geophysical Research Letters

RESEARCH LETTER
10.1029/2025GL120608

Constraints on Past CO_2 and Climate Sensitivity From Global Temperature and Sea Level Reconstructions Across the Plio-Pleistocene

Peter Köhler[1] **and Peter U. Clark**[2,3]

[1]Alfred-Wegener-Institut Helmholtz-Zentrum für Polar-und Meeresforschung, Bremerhaven, Germany, [2]College of Earth, Ocean, and Atmospheric Sciences, Oregon State University, Corvallis, OR, USA, [3]School of Geography and Environmental Sciences, University of Ulster, Coleraine, UK

Key Points:

- New temperature and global mean sea level data since 4.5 Ma with large ice-sheet variability throughout the Pleistocene force C cycle model
- Energy balance requires that simulated atmospheric CO_2 concentration before 2 Ma must be 300–450 ppm to best agree with climate data
- After accounting for missing forcings and feedbacks our results for the past 4 Myr suggest that equilibrium climate sensitivity is 1.8–1.9 K

Supporting Information:

Supporting Information may be found in the online version of this article.

Correspondence to:

P. Köhler,
peter.koehler@awi.de

Citation:

Köhler, P., & Clark, P. U. (2026). Constraints on past CO_2 and climate sensitivity from global temperature and sea level reconstructions across the Plio-Pleistocene. *Geophysical Research Letters*, *53*, e2025GL120608. https://doi.org/10.1029/2025GL120608

Received 11 NOV 2025
Accepted 15 FEB 2026

Author Contributions:

Conceptualization: Peter Köhler, Peter U. Clark
Data curation: Peter Köhler
Formal analysis: Peter Köhler
Funding acquisition: Peter U. Clark
Investigation: Peter Köhler
Methodology: Peter Köhler
Software: Peter Köhler
Validation: Peter Köhler
Visualization: Peter Köhler
Writing – original draft: Peter Köhler, Peter U. Clark
Writing – review & editing: Peter Köhler, Peter U. Clark

Abstract In contrast to previous approaches, new reconstructions of changes in global mean surface temperature and global mean sea level (GMSL) include large variability in GMSL throughout the Pleistocene. Here we assess these reconstructions from an energy balance perspective by using them to force a global carbon cycle model in different scenarios that capture the spread in existing CO_2 reconstructions. Results suggests that a high CO_2 scenario (300–450 ppm before 2 million years ago) is most consistent with the new climate reconstructions. When radiative forcing from the high CO_2 scenario and land-ice albedo derived from the new GMSL reconstruction are corrected for other forcings and feedbacks, but ignoring any state-dependency, these results for the past 4 million years suggest an equilibrium climate sensitivity of 1.8–1.9 K which is just below the 5%–95% confidence range of recent estimates using other approaches (2.1–4.0 K).

Plain Language Summary Most reconstructions of global mean sea level (GMSL) change show an increase in amplitude together with a decrease in frequency across the Mid-Pleistocene transition around 1 million years ago. A new reconstruction now suggests that large changes of sea level occurred throughout the last 2.5 million years. Here we use both newly reconstructed temperature and sea level to force a global carbon cycle model over the past 4 million years and simulate changes in atmospheric CO_2 concentration. When Earth is in energy balance, temperature change reflects the sum of the main contributors of radiative forcing changes: the greenhouse effect of atmospheric CO_2 and Earth's reflectivity, whose main component is caused by ice sheet coverage, which can be estimated from GMSL change. We find that a high CO_2 scenario (300–450 ppm before 2 million years ago) delivers most consistent results. When radiative forcing is corrected for missing forcings and feedbacks, we use our results to calculate a temperature rise of 1.8–1.9°C for a CO_2 doubling, referred to as equilibrium climate sensitivity. This result is slightly lower than the range given by other recent approaches.

1. Introduction

Our understanding of Cenozoic climate change is commonly based on changes in the $\delta^{18}O$ of calcite shells of benthic foraminifera $(\delta^{18}O_b)$ that record some combination of the temperature-dependent isotopic fractionation during calcite formation and the $\delta^{18}O$ of sea water $(\delta^{18}O_{sw})$ that largely reflects ice volume (e.g., Emiliani, 1955; Lisiecki & Raymo, 2005; Westerhold et al., 2020). The longstanding inference from the $\delta^{18}O_b$ record of the past 4.5 million years (Myr) is that changes in mean ocean temperature (MOT) and global mean sea level (GMSL) jointly experienced two transitions toward larger fluctuations (Hansen et al., 2013; Raymo, 1994; Rohling et al., 2022). Here, GMSL covers only the barystatic effect introducing a small bias of less than 3 m by the omission of the thermostatic component of about 0.7 m per K change in MOT (Hieronymus, 2019). The first transition occurred between 3 and 2.5 million years ago (Ma) and represents increasingly colder temperatures and larger Northern Hemisphere ice sheets both of which fluctuated with a 41-thousand-year (kyr) periodicity. The second Mid Pleistocene transition (MPT) that occurred ~1 Ma is characterized by even larger fluctuations of MOT and Northern Hemisphere ice sheets with an accompanying change from a dominant 41-kyr periodicity to a dominant 100-kyr periodicity.

Recent studies, however, suggest that several additional factors may also have influenced $\delta^{18}O_b$ records, leading to a reevaluation of late Cenozoic climate and sea-level evolution. For example, Meckler et al. (2022) found that deep ocean temperature estimates based on clumped isotopes over the past 65 Myr are higher than estimates derived from

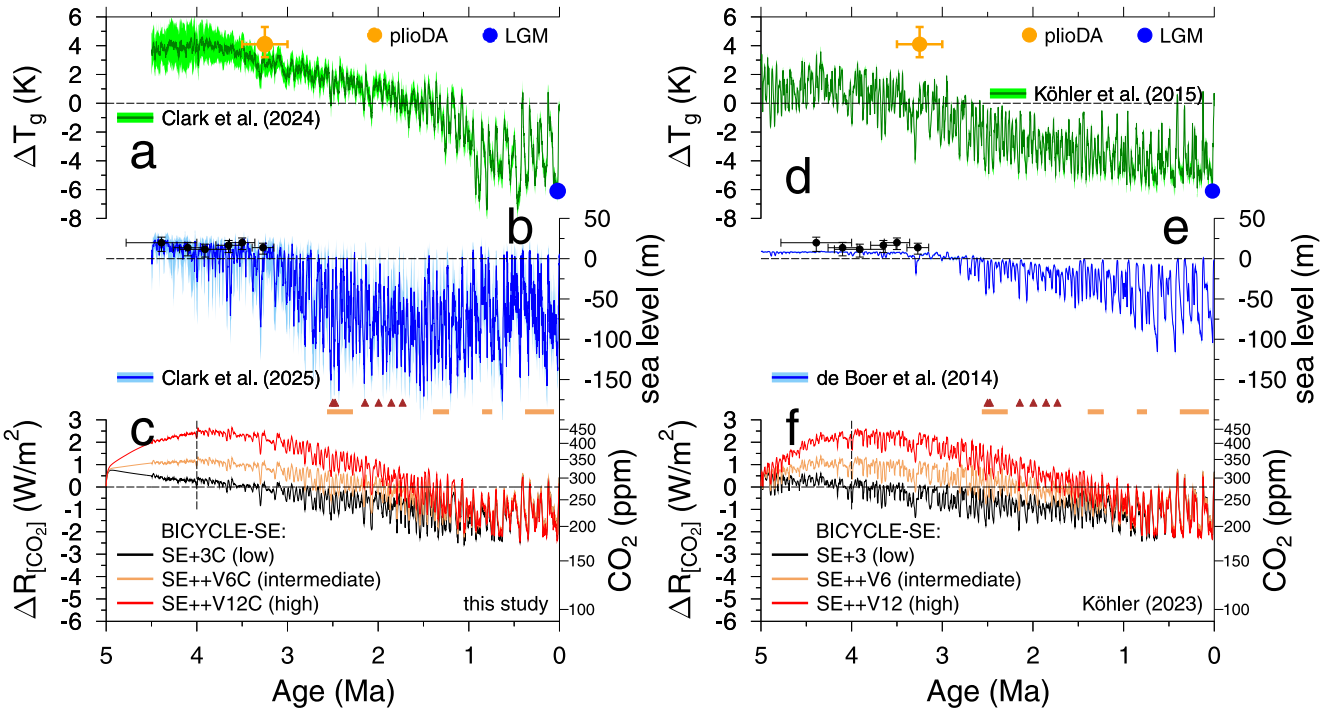

Figure 1. New (left) and examples of previous (right) understanding of Plio-Pleistocene climate change. Left: (a) ΔT_g of CL1 and (b) global mean sea level (GMSL) of CL3 as used here to simulate (c) atmospheric CO_2. Right: (d) ΔT_g of Köhler et al. (2015) and (e) GMSL of de Boer et al. (2014) as used in Köhler (2023) to simulate (f) atmospheric CO_2. Time series of ΔT_g and GMSL include independent examples of reconstructed changes: ΔT_g at Last Glacial Maximum (blue circles, Tierney et al., 2020), ΔT_g at the mid-Pliocene (95% CI at 3.5–3.0 Ma from plioDA, orange circles, Tierney et al., 2025), sea level highstands from Mallorcan speleothem (black circles, Dumitru et al., 2019) and indications for large Laurentide ice sheets, for example, Mississippi outflow (brown triangles, Shakun et al., 2016) and indications of ice sheets extending as far south as 39°N (light brown bars, Balco & Rovey, 2010). Simulated CO_2 time series are used only after 4 Ma (vertical line) since they are perturbed by spin-up effects before.

$\delta^{18}O_b$ (Rohling et al., 2024), suggesting long-term changes in deep-ocean pH or $\delta^{18}O_{sw}$. An alternative decomposition of $\delta^{18}O_b$ based on Mg/Ca temperature reconstructions (Miller et al., 2024) is in better agreement with Meckler et al. (2022), but still points to open questions in fully understanding $\delta^{18}O_b$. Clark, Shakun, Rosenthal, Pollard, et al. (2025) (hereafter CL3) reconstructed GMSL for the past 4.5 Myr by subtracting the change in MOT (ΔMOT, relative to preindustrial) from a $\delta^{18}O_b$ stack (Ahn et al., 2017) that required a change in the relationship between MOT and global mean sea surface temperature (GMSST) prior to 1 Ma (Clark, Shakun, Rosenthal, Zhu, et al., 2025) (hereafter CL2). They also removed a long-term trend from $\delta^{18}O_b$ that is likely due to diagenetic or carbonate-ion effects (Raymo et al., 2018) as well as accounted for the time-varying temperature effects on the $\delta^{18}O$ of ice sheets and thus $\delta^{18}O_{sw}$. As a result, their GMSL reconstruction differs (mainly due to the used MOT and the corrected $\delta^{18}O_b$ records) from previous studies that did not account for these effects (e.g., Hansen et al., 2013; Rohling et al., 2022). In particular, they found that although global mean surface temperature change (ΔT_g) (Clark et al., 2024) (hereafter CL1), ΔMOT, and GMSL are characterized by a change from dominant 41-kyr periodicity to dominant 100-kyr periodicity across the MPT, only ΔT_g and ΔMOT show an increase in the amplitude of the fluctuations while GMSL experienced large fluctuations throughout the Pleistocene (Figures 1a and 1b). It's important to note that (a) early Pleistocene and Pliocene GMSL lowstands would be even lower than in CL3 if there was no change in MOT scaling with GMSST or no removal of a long-term trend and (b) early Pleistocene lowstands remained below −100 m even with 5–10 times the glacial-interglacial variability that was used. This led CL3 to conclude that "the finding of LGM-like sea-level lowstands during the early Pleistocene is robust across a wide range of parameter values in our model and is consistent with several lines of geological evidence." Thus, all previous hypotheses that explained the periodicity change in GMSL during the MPT by a change in the sensitivity of Northern Hemisphere ice sheets to orbital forcing through an increase in their volume (e.g., Figure 1e; Barker et al., 2025; Bintanja & van de Wal, 2008; Clark & Pollard, 1998; Clark et al., 2006; Huybers, 2006; Köhler & van de Wal, 2020; Tzedakis et al., 2017; Willeit et al., 2019) are no longer supported by the new GMSL reconstruction.

These new climate time series (ΔT_g, ΔMOT, and GMSL from CL1, CL2, and CL3) are depending on each other and therefore should be interpreted as a whole. Potential future revisions of the underlying sea surface temperature (SST) data would lead to subsequent changes in all data sets.

CL3 discussed several challenges posed by the new ΔT_g and GMSL reconstructions, including large changes in sea level that occurred throughout the Pleistocene rather than temperature varying with ice volume as the Earth cooled. This is perhaps best illustrated by the interval between about 2.5 and 1 Ma when GMSL during glacial maxima was within the uncertainties about as low as at the Last Glacial Maximum (LGM) while ΔT_g during peak glacials was never lower than about half of the −6 K reconstructed for the LGM and even higher than preindustrial temperatures earlier in this time interval (Figures 1a and 1b). While this relationship of low GMSL at relatively high surface temperatures is still not completely understood, a recent study identified a state-dependent ice-sheet response with opposing effects for warm and cold climate states (Golledge et al., 2026). Here we address this challenge by assessing whether the new ΔT_g reconstruction can be reconciled with the radiative forcing from atmospheric CO_2 concentration and ice-sheet albedo derived from the new GMSL reconstruction, the two largest contributing processes to the global energy imbalance. Given the large spread in CO_2 reconstructions prior to the ice-core record of the past 800 kyr, we use several scenarios based on simulated CO_2 that encompass the range seen in the data (Köhler, 2023), allowing us to determine from an energy balance perspective those CO_2 levels that are most consistent with the new ΔT_g and GMSL reconstructions and calculate the associated climate sensitivity. Forthcoming older CO_2 data from ongoing ice core projects might further constrain the most reasonable combination of Pleistocene climate records.

2. Plio-Pleistocene Atmospheric CO_2

The Cenozoic CO_2 Proxy Integration Project ($CenCO_2PIP$) Consortium (2023) compiled and assessed the full range of the proxy-based reconstructions of Cenozoic atmospheric CO_2 concentrations and then constructed a time series of CO_2 based only on the best constrained data and their uncertainties. Köhler (2023) focused on CO_2 estimates based on $\delta^{11}B$ measured in planktonic foraminifera. He used the carbon cycle box model BICYCLE-SE to derive time series of atmospheric CO_2 concentration and of various variables of the marine carbonate chemistry (e.g., pH, alkalinity) and assessed assumptions made in the $\delta^{11}B$-based CO_2 proxy. For our current study, we use both simulated and proxy-based CO_2 data from Köhler (2023), but similar insights are also possible when using the $CenCO_2PIP$ compilation, since the proxy-based CO_2 data sets are based on the same measurements. For reasons given in Köhler (2023), we neglect alkenone-based CO_2 and some questionable $\delta^{11}B$-based data sets (Guillermic et al., 2022; Seki et al., 2010), but add CO_2 reconstructions from leaf wax $\delta^{13}C$ (Yamamoto et al., 2022) and paleosols (Da et al., 2019, 2025) to the $\delta^{11}B$-based results as updated in Dyez et al. (2018) and de la Vega et al. (2020) and initially published elsewhere (Bartoli et al., 2011; Chalk et al., 2017; Hönisch et al., 2009; Martínez-Botí et al., 2015) which extended the 0.8 Myr long CO_2 record from ice cores (Bereiter et al., 2015) and the 2 Myr old snapshots from blue ice (Yan et al., 2019). This compilation gives a wide range of CO_2 concentrations, with paleosol data having particularly large uncertainties (Figure S1 in Supporting Information S1). Because the range of CO_2 at any particular time cannot be as large as the spread in the data (Köhler, 2023), we assume they contain proxy- or lab-specific effects that have not yet been corrected for. We address this uncertainty by dividing the CO_2 proxy data into two subsets, with the primary distinction being those data from 2 to 4 Ma with CO_2 values mainly <300 ppm (subset of low CO_2, Figure S1a in Supporting Information S1) and those with CO_2 values mainly >300 ppm (subset of intermediate to high CO_2, Figure S1b in Supporting Information S1). However, for this split we keep results of individual approaches together in either one of the subsets; for example, all data from Bartoli et al. (2011) were allocated to the low CO_2 subset, although some CO_2 data points above 300 ppm between 2 and 4 Ma are contained therein.

Köhler (2023) found that simulations with BICYCLE-SE can explain both low and high CO_2 depending on the assumed changes in weathering and volcanic CO_2 outgassing. Since these simulations were based on earlier reconstructions of ΔT_g and GMSL, we now repeat these scenarios using the new SST, ΔT_g, MOT, and GMSL reconstructions from CL1, CL2, and CL3. Simulations with BICYCLE-SE all start from preindustrial conditions. Because assumed volcanic CO_2 outgassing rates in the intermediate and high CO_2 scenarios are larger than today, the carbon cycle needs about 1 Myr for equilibration (Köhler, 2023). Thus, our new simulations start at 5 Ma having 0.5 Myr of spin-up for climate conditions at 4.5 Ma, but simulation results are used only after 4 Ma for further analysis. Changes in SST have been divided at 30°N/S and are used to prescribe SST in either the

respective high latitude polar or low latitude surface boxes, deep ocean temperature is prescribed by MOT, and the terrestrial carbon cycle depends on ΔT_g (see Figure S2 in Supporting Information S1). The SST data base from CL1 has no data before 1 Ma south of 45°S, implying that the prescribed Southern Ocean SST there is based only on data between 30 and 45°S. However, these data contain no southern polar amplification for the warmer than preindustrial part of the Plio-Pleistocene (Figure S2b in Supporting Information S1), while such an amplification is contained in a data assimilation for the Pliocene (Tierney et al., 2025). To test the importance of this omission, we substitute Southern Ocean SST changes with northern high-latitude SST data which contain the polar amplification throughout the investigated time window (Figure S2b in Supporting Information S1). The simulated atmospheric CO_2 concentrations based on this revised SST forcing differ in the 2–4 Ma time window by 0.9 ± 3.4 (1σ) ppm from the baseline, suggesting that the imperfect Southern Ocean SST forcing is only a minor uncertainty of our approach.

While the new and old CO_2 simulations differ in detail, with smaller glacial-interglacial amplitudes when based on the new reconstructions before 2.5 Ma, the overall dynamics after 2.5 Ma for a given scenario are largely the same (Figures 1c and 1f), implying that the impacts of the revised temperatures and GMSL largely compensate each other. Because such compensation is unexpected when considering just the individual effects of SST and GMSL on simulated atmospheric CO_2 (Köhler & Munhoven, 2020), it likely reflects the combination of subsequent carbon cycle effects, for example, SST changes in the North Atlantic induce changes in the Atlantic meridional overturning circulation (Figure S3b in Supporting Information S1), high latitude SST determines sea ice coverage (Figure S3d in Supporting Information S1), and GMSL changes drive Southern Ocean vertical mixing (Figure S3c in Supporting Information S1) and coral reef growth, all of which also contribute to changes in the carbon cycle (Köhler, 2023).

3. Implications for Global Energy Balance

Figure 1 compares the ΔT_g, GMSL, and simulated CO_2 reconstructions used for our new energy balance assessment with an example of previously used reconstructions (de Boer et al., 2014; Köhler, 2023; Köhler et al., 2015). Examples of independent data constraints on extremes are also included in Figure 1 giving indications of the shortcomings, especially of GMSL, in the previous approaches. See CL1 and CL3 for further discussions. Although our focus is on the new reconstructions, we also provide in Figures S5 and S6 in Supporting Information S1 results to illustrate the previous approaches.

The forcing related to global temperature change on orbital timescales (Köhler et al., 2010) is dominated by the radiative forcing of atmospheric CO_2,

$$\Delta R_{[CO_2]} = 5.35\ \mathrm{W/m^2} \cdot \ln\left(\frac{CO_2}{278\ \mathrm{ppm}}\right) \quad (1)$$

(Myhre et al., 1998) and the land ice (LI) albedo $\Delta R_{[LI]}$, which can be calculated from 3D ice-sheet models (de Boer et al., 2014). We approximate $\Delta R_{[LI]}$ from GMSL (Figure S4 in Supporting Information S1) following the results used in a previous approach (Köhler et al., 2015). Although this older study contains lower GMSL variability during the early Pleistocene than the new GMSL reconstruction, the embedded non-linear relationship between albedo and GMSL derived from the ANICE ice-sheet model is a robust feature which is independent from the temporal dynamics of the model. The third-order polynomial between GMSL and $\Delta R_{[LI]}$ gives the most reasonable results, although the model range of −120 to +10 m GMSL is smaller than in the new GMSL reconstruction making this approximation subject to possible errors when extrapolating our fitting function to GMSL changes below −120 and above +10 m. Previous studies (e.g.., Hansen et al., 2008; Martínez-Botí et al., 2015) used a linear relation of

$$\Delta R_{[LI]} = 0.0308\ \mathrm{W/m^3} \cdot \mathrm{GMSL} \quad (2)$$

which we plot for comparison in Figure S4 in Supporting Information S1. Whatever form it takes, this transfer function from GMSL to $\Delta R_{[LI]}$ oversimplifies the system especially for intermediate GMSL lowstands where the width of the related $\Delta R_{[LI]}$ of about 2 W/m^2 is collapsing into a single number (Figure S4 in Supporting Information S1). In other words, in the ice sheet model, different land ice areal extents exist for the same ice volume

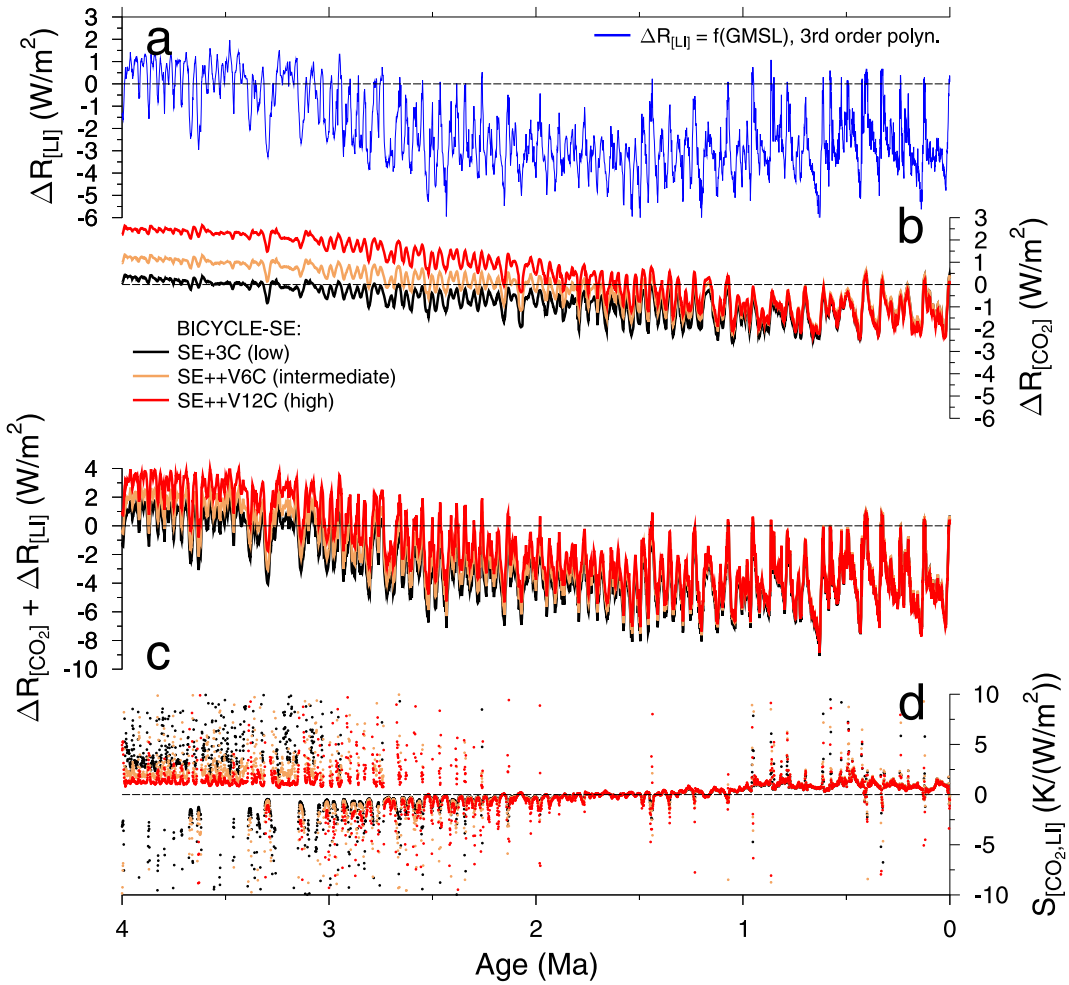

Figure 2. Radiative forcing when using CO_2 simulations based on the new climate reconstructions (CL1, CL2, and CL3). (a) Land ice albedo radiative forcing $\left(\Delta R_{[LI]}\right)$ calculated from global mean sea level (Figure S4 in Supporting Information S1). (b) Radiative forcing of CO_2 ($\Delta R_{[CO_2]}$) based on the noted simulation scenarios using BICYCLE-SE. (c) Summed forcing of $\Delta R_{[CO_2]} + \Delta R_{[LI]}$. (d) Pointwise specific climate sensitivity $S_{[CO_2,LI]}$ following Equation 3. Colorcode in panel (b) is also applied in panels (c, d).

or GMSL. As previously found by Köhler et al. (2015), the $\Delta R_{[LI]}$-GMSL relationship is nearly linear for deglaciations and non-linear for glacial inceptions with the difference reflecting initial ice buildup that is extending into the area before ice sheet height (or volume gain) is achieved. Note that this approach only considers the albedo effect of ice sheets on the shortwave radiation while topography or dynamics effects (e.g., Zhu & Poulsen, 2021) are ignored.

The efficacy (ε) of land ice albedo, that is the importance of $\Delta R_{[LI]}$ relative to $\Delta R_{[CO_2]}$ for the resulting temperature change (Hansen et al., 2005), has recently been a focus of discussion. One study using an Earth system model of intermediate complexity over the last 5 Myr suggests ε is 0.45 (Stap et al., 2019), implying that $\Delta R_{[CO_2]}$ is about twice as important as $\Delta R_{[LI]}$ for a given amount of radiative forcing. However, other more complex models applied over certain paleo time slices suggest that ε might be >1 and also depend on climate state (e.g., Cooper et al., 2024; Zhu & Poulsen, 2021) and relate efficacy to the pattern effect (Zhou et al., 2023). For reasons of simplicity, we ignore changes in efficacy here ($\varepsilon = 1$) partly because any state-dependency of our analysis has already been biased by the calculation of $\Delta R_{[LI]}$ out of GMSL.

We combine these assumptions to derive individual and summed radiative forcing that varies between +4 and −8 W/m^2 over the past 4 Myr when based on the new data (Figure 2) or between +3 and −6 W/m^2 in the previous

approach (Figure S5 in Supporting Information S1). When plotted pointwise on 1-kyr time steps, the specific climate sensitivity (PALAEOSENS-Project Members, 2012)

$$S_{[CO_2,LI]} = \frac{\Delta T_g}{\Delta R_{[CO_2]} + \Delta R_{[LI]}} \quad (3)$$

gives a first overview of the analyzed system (Figure 2d and Figure S5d in Supporting Information S1). If $S_{[CO_2,LI]} < 0$ K/(W/m^2), the considered forcing and temperature response have opposite sign, indicating that other important forcings and feedbacks not linearly related to those applied here are missing, that the system is not in equilibrium, or the system is in an unrealistic state. Figure 2d shows that for the new data, the low CO_2 scenario accounts for 44% of $S_{[CO_2,LI]} < 0$ K/(W/m^2) over the past 4 Myr (mainly between 1.5 and 3 Ma) suggesting an unrealistic combination of forcing and temperature change. The results contain fewer data points with $S_{[CO_2,LI]}$ below 0 K/(W/m^2) for the intermediate (38%) and for the high CO_2 simulations (32%). For previous reconstructions of ΔT_g and $\Delta R_{[LI]}$ (Figure S5d in Supporting Information S1), the low CO_2 scenario accounts for 4% of $S_{[CO_2,LI]} < 0$ K/(W/m^2) over the past 4 Myr, whereas $S_{[CO_2,LI]} < 0$ K/(W/m^2) accounts for 20% and 32% of the data points for the intermediate and high CO_2 simulations, respectively (primarily between 2 and 3.5 Ma), again pointing to a more unrealistic combination of these latter two time series.

As described elsewhere (Köhler et al., 2017), the specific climate sensitivity $S_{[X]}$ can be calculated from the slope of the regression through the ΔT_g data versus the considered forcing $\Delta R_{[X]}$, ideally with the regression intersecting the origin (i.e., no temperature effect for no forcing), if $S_{[X]}$ is independent of climate state. However, a non-linear regression that provides a better fit to the data indicates a state-dependent behavior for $S_{[X]}$, in which case a quantification of specific climate sensitivity should be based on the analysis of $S_{[X]}$ as function of $\Delta R_{[X]}$.

Scatterplots of temperature against forcing for the previous reconstructions suggest that $S_{[CO_2,LI]}$ is state dependent since the second-order polynomials approximate the data with higher r^2 than the linear regressions (Figure S6 in Supporting Information S1). Here, results based on binned data to overcome any uneven distribution of the data yield slightly better regression coefficients. This finding confirms previous results which have been derived from proxy-based CO_2 and not from simulated CO_2 (Köhler et al., 2015). The authors also found that the dominant part of this state-dependency is caused by using a 3D ice sheet model for the calculation of $\Delta R_{[LI]}$. Further analysis on climate sensitivity based on the previous approach is due to this state-dependency being more complex and not performed here since our focus is on the new reconstructions, but see Köhler et al. (2017) for the past 2.1 Myr, when CO_2 is based on one specific set of proxy data.

Since a 3D ice sheet model is not applied when our analysis is based on the new reconstructions, the corresponding scatterplots are not tested for state-dependency (Figures 3a–3c). Furthermore, as already mentioned above, temperature and forcing anomalies should at best have the same sign, avoiding a population of the scatterplots with data of opposite signs (gray shaded quadrants in upper left and lower right in Figure 3 and Figure S6 in Supporting Information S1). On this basis, we can see a shift of the data and a narrowing of their spread in the new reconstructions for scenarios with increasing CO_2 concentrations (Figure 3) as opposed to a shift of the data and a narrowing of their spread in the previous reconstructions for scenarios with decreasing CO_2 concentrations (Figure S6 in Supporting Information S1).

The most likely combination of the new ΔT_g and GMSL reconstructions and a high atmospheric CO_2 scenario suggests that for the past 4 Myr, the specific climate sensitivity $S_{[CO_2,LI]}$ was 0.8 K/(W/m^2) (Figure 3c). From this, we can derive S^a (where "a" stands for actuo, see PALAEOSENS-Project Members (2012) for further details) if we correct for missing greenhouse gas forcings of CH_4 and N_2O and feedbacks of vegetation and aerosols. S^a can then be used to calculate the equilibrium climate sensitivity (ECS), the expected long-term global mean warming caused by CO_2 doubling in the modern climate typically derived from state-of-the-art climate models, if multiplied by the corresponding radiative forcing of $\Delta R_{[2\times CO_2]}$ of 3.71 W/m^2 directly derived from Equation 1.

We estimate an amplification factor α for $\Delta R_{[CO_2]}$ that accounts for the missing forcings and feedbacks by using the 800-kyr long data compilation of Köhler et al. (2010) under the assumptions of an efficacy of 1 in all these additional effects and a possible extrapolation of the gained relationship beyond this time window covered by ice

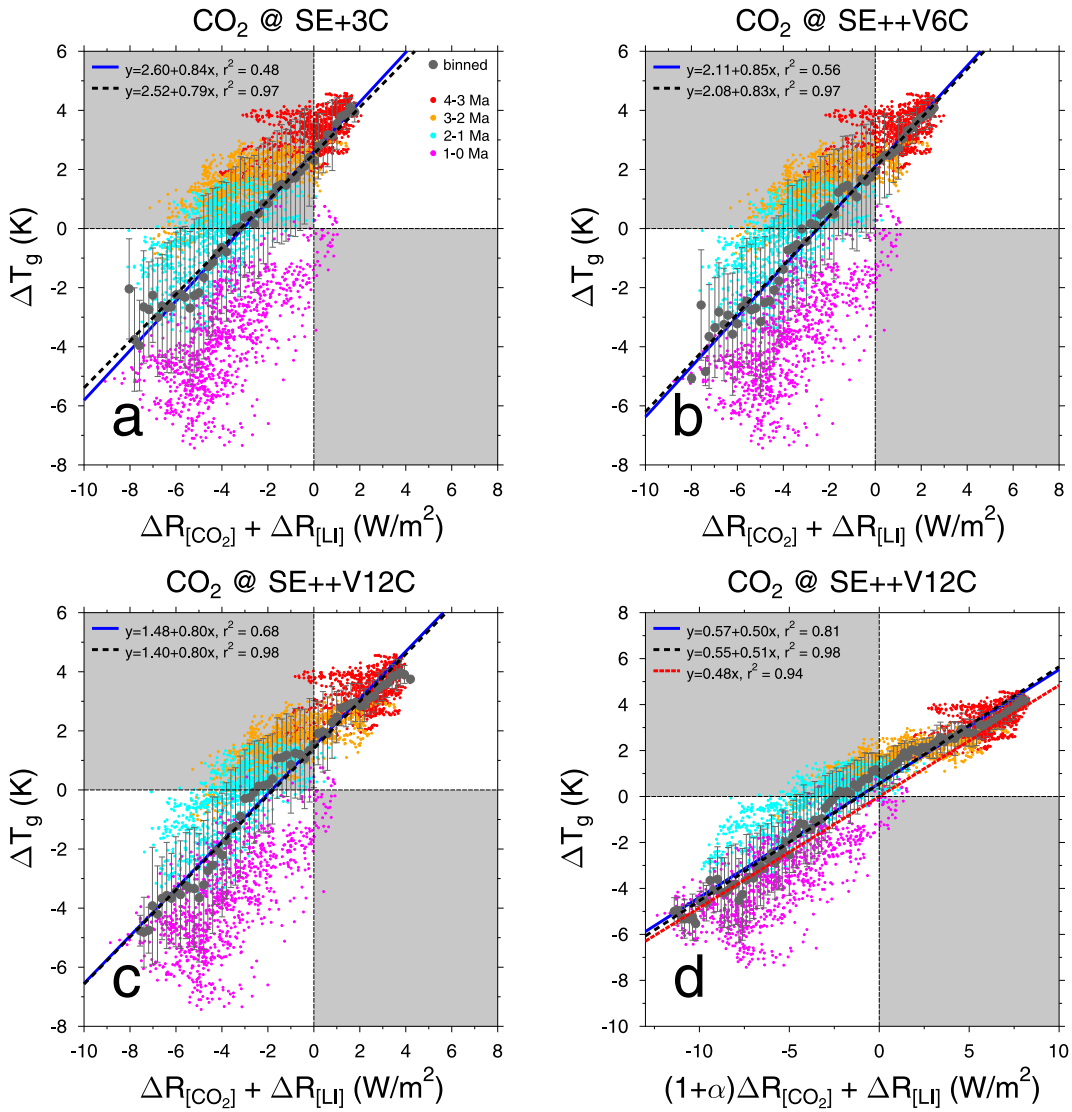

Figure 3. Scatterplots of ΔT_g versus radiative forcing based on the past 4 Ma of the new climate reconstructions (CL1, CL2, and CL3). (a–c) Radiative forcing of $\Delta R_{[CO_2]} + \Delta R_{[LI]}$. The applied CO_2 in different subpanels is taken from the simulation scenario mentioned in the headings. (d) Radiative forcing of $(1 + \alpha)\Delta R_{[CO_2]} + \Delta R_{[LI]}$ with $\alpha = 1.66$ correcting for other forcings and feedbacks for the preferable combination of data sets (high CO_2 scenario SE++V12C). Original data (one point each 1 kyr, colorcoded by time, see legend in panel (a)) are averaged in bins in ΔR of 0.2 W/m^2 width (dark gray circles with $\pm 1\sigma$). Regressions are either using the original (blue line) or the binned (black broken line) data. Gray shaded areas are those in which ΔT_g and ΔR have the opposite sign. Variables in these areas might be possible due to various feedbacks, but more naturally data should preferably fall in the white quadrants.

core data. Ignoring uncertainties in all these data gives $\alpha = 1.66$ (Figure S7 in Supporting Information S1), which, if used in Equation 4,

$$S^a = \frac{\Delta T_g}{(1+\alpha)\cdot \Delta R_{[CO_2]} + \Delta R_{[LI]}}, \tag{4}$$

leads to S^a of 0.48–0.51 K/(W/m^2) depending as to whether the regressions are forced through the origin or not (Figure 3d), corresponding to an ECS of 1.8–1.9 K.

Our results are just slightly below the 5%–95% confidence range for ECS of 2.1–4.0 K from recent studies using paleo data and models for the LGM (Cooper et al., 2024) and the Pliocene (Cooper et al., 2026) that included

differences in feedbacks between the climate state and a future CO_2 doubling (the pattern effect). The new studies revised an earlier community-wide effort on ECS (Sherwood et al., 2020) that combined several lines of evidence, feedback process understanding, and the historical and paleoclimate records which led to a 5%–95% range in ECS of 2.3–4.7 K. Note that different efficacies of the forcing were also not considered in earlier approaches (e.g., PALAEOSENS-Project Members, 2012) and it entered the ECS estimates in Sherwood et al. (2020) only as uncertainties. We do not consider further uncertainty evaluations for S^a or ECS particularly since the transformation of GMSL into $\Delta R_{[LI]}$ was a major simplification with no associated uncertainty that already led to the disappearance of any potential state-dependency in S^a. Such a previously noted state-dependency of S^a (e.g., Köhler et al., 2017) with higher values during warmer climates would partly be compensated by the pattern effect, which corrected the climate feedback parameter $\lambda = -1/S^a$ by $\Delta\lambda$ before calculating ECS after

$$\mathrm{ECS} = \frac{-\Delta R_{[2\times CO_2]}}{\lambda + \Delta\lambda}. \quad (5)$$

Here, $\Delta\lambda$ was found to be around -0.4 (W/m^2)/K for both the cold LGM and the warm Pliocene (Cooper et al., 2024, 2026). However, we are aware that an efficacy of the land ice forcing different from 1 would impact our estimated ECS. For example, if we use $\varepsilon = 0.45$ (Stap et al., 2019) we would obtain an ECS of 2.3 K, while $\varepsilon > 1$ as suggested by others would result in an ECS even smaller than our current result, further away from the findings of others. We have thus primarily demonstrated that the new ΔT_g and GMSL reconstructions are consistent with our current understanding of climate sensitivity approximated from paleodata assuming past high CO_2 concentrations.

4. Conclusions

We forced a carbon cycle model with new temperature and GMSL reconstructions for the past 4.5 Myr (CL1, CL2, and CL3). Based on different assumptions regarding volcanism and weathering, the simulated atmospheric CO_2 concentrations are either low (<300 ppm) or intermediate to high (>300 ppm) at 2–4 Ma. Both results can be supported by different CO_2 reconstructions. Using ΔT_g, GMSL and CO_2 in an energy balance perspective, we find that the new reconstructions are more consistent with the higher CO_2 scenario while previous reconstructions are more consistent with the lower CO_2 scenario. Forthcoming ice core-based CO_2 data extending beyond the past 800 kyr (Chung et al., 2023) may thus distinguish between the different ΔT_g and GMSL reconstructions. Equilibrium climate sensitivity for CO_2 doubling calculated from the high CO_2 scenario with the new reconstructions over the past 4 Myr is 1.8–1.9 K, slightly lower than the 5%–95% confidence range found by other recent approaches.

Conflict of Interest

The authors declare no conflicts of interest relevant to this study.

Data Availability Statement

Regional SST, important model forcing time series and simulated atmospheric CO_2 are available in Köhler and Clark (2026). Input data and simulation output from the previous approaches are listed in Köhler (2023). The model as used here is—apart from the mentioned update of used climate forcing based on temperature and GMSL—completely described in Köhler (2023).

Acknowledgments
This publication contributed to Beyond EPICA, a project of the European Union's Horizon 2020 Research and Innovation Program (Oldest Ice Core). This is Beyond EPICA Publication 48. PUC acknowledges funding from the National Science Foundation (OPP-2103032). We thank W. John Schmelz and an anonymous reviewer for comments. Open Access funding enabled and organized by Projekt DEAL.

References

Ahn, S., Khider, D., Lisiecki, L. E., & Lawrence, C. E. (2017). A probabilistic Pliocene-Pleistocene stack of benthic $\delta^{18}O$ using a profile hidden Markov model. *Dynamics and Statistics of the Climate System*, *2*(1), dzx002. https://doi.org/10.1093/climsys/dzx002

Balco, G., & Rovey, C. W. II. (2010). Absolute chronology for major Pleistocene advances of the Laurentide ice sheet. *Geology*, *38*(9), 795–798. https://doi.org/10.1130/G30946.1

Barker, S., Lisiecki, L. E., Knorr, G., Nuber, S., & Tzedakis, P. C. (2025). Distinct roles for precession, obliquity, and eccentricity in Pleistocene 100-kyr glacial cycles. *Science*, *387*(6737), eadp3491. https://doi.org/10.1126/science.adp3491

Bartoli, G., Hönisch, B., & Zeebe, R. E. (2011). Atmospheric CO_2 decline during the Pliocene intensification of Northern Hemisphere glaciations. *Paleoceanography*, *26*(4), PA4213. https://doi.org/10.1029/2010PA002055

Bereiter, B., Eggleston, S., Schmitt, J., Nehrbass-Ahles, C., Stocker, T. F., Fischer, H., et al. (2015). Revision of the EPICA Dome C CO_2 record from 800 to 600 kyr before present. *Geophysical Research Letters*, *42*(2), 542–549. https://doi.org/10.1002/2014GL061957

Bintanja, R., & van de Wal, R. S. W. (2008). North American ice-sheet dynamics and the onset of the 100,000-year glacial cycles. *Nature*, *454*(7206), 869–872. https://doi.org/10.1038/nature07158

The Cenozoic CO_2 Proxy Integration Project ($CenCO_2PIP$) Consortium. (2023). Toward a Cenozoic history of atmospheric CO_2. *Science*, *382*(6675), eadi5177. https://doi.org/10.1126/science.adi5177

Chalk, T. B., Hain, M. P., Foster, G. L., Rohling, E. J., Sexton, P. F., Badger, M. P. S., et al. (2017). Causes of ice age intensification across the mid-Pleistocene transition. *Proceedings of the National Academy of Sciences of the United States of America*, *114*(50), 13114–13119. https://doi.org/10.1073/pnas.1702143114

Chung, A., Parrenin, F., Steinhage, D., Mulvaney, R., Martín, C., Cavitte, M. G. P., et al. (2023). Stagnant ice and age modelling in the Dome C region, Antarctica. *The Cryosphere*, *17*(8), 3461–3483. https://doi.org/10.5194/tc-17-3461-2023

Clark, P. U., Archer, D., Pollard, D., Blum, J. D., Rial, J. A., Brovkin, V., et al. (2006). The middle Pleistocene transition: Characteristics, mechanisms, and implications for long-term changes in atmospheric CO_2. *Quaternary Science Reviews*, *25*(23–24), 3150–3184. https://doi.org/10.1016/j.quascirev.2006.07.008

Clark, P. U., & Pollard, D. (1998). Origin of the middle Pleistocene transition by ice sheet erosion of regolith. *Paleoceanography*, *13*(1), 1–9. https://doi.org/10.1029/97PA02660

Clark, P. U., Shakun, J. D., Rosenthal, Y., Köhler, P., & Bartlein, P. J. (2024). Global and regional temperature change over the past 4.5 million years. *Science*, *383*(6685), 884–890. https://doi.org/10.1126/science.adi1908

Clark, P. U., Shakun, J. D., Rosenthal, Y., Pollard, D., Hostetler, S. W., Köhler, P., et al. (2025). Global mean sea level over the past 4.5 million years. *Science*, *390*(6770), eadv8389. https://doi.org/10.1126/science.adv8389

Clark, P. U., Shakun, J. D., Rosenthal, Y., Zhu, C., Gregory, J. M., Köhler, P., et al. (2025). Mean ocean temperature change and decomposition of the benthic $\delta^{18}O$ record over the last 4.5 million years. *Climate of the Past*, *21*(6), 973–1000. https://doi.org/10.5194/cp-21-973-2025

Cooper, V. T., Armour, K. C., Hakim, G. J., Tierney, J. E., Burls, N. J., Proistosescu, C., et al. (2026). Paleoclimate pattern effects help constrain climate sensitivity and 21st-century warming. *Proceedings of the National Academy of Sciences*, *123*(4), e2511370123. https://doi.org/10.1073/pnas.2511370123

Cooper, V. T., Armour, K. C., Hakim, G. J., Tierney, J. E., Osman, M. B., Proistosescu, C., et al. (2024). Last Glacial Maximum pattern effects reduce climate sensitivity estimates. *Science Advances*, *10*(16), eadk9461. https://doi.org/10.1126/sciadv.adk9461

Da, J., Zhang, Y. G., Li, G., Meng, X., & Ji, J. (2019). Low CO_2 levels of the entire Pleistocene epoch. *Nature Communications*, *10*(1), 4342. https://doi.org/10.1038/s41467-019-12357-5

Da, J., Zhang, Y. G., Liu, X., Breecker, D. O., Li, G. K., Chen, T., & Ji, J. (2025). No apparent state-dependency of equilibrium climate sensitivity between the Pleistocene glacial and interglacial climate states. *Nature Communications*, *16*(1), 6608. https://doi.org/10.1038/s41467-025-61941-5

de Boer, B., Lourens, L. J., & van de Wal, R. S. (2014). Persistent 400,000-year variability of Antarctic ice volume and the carbon cycle is revealed throughout the Plio-Pleistocene. *Nature Communications*, *5*(1), 2999. https://doi.org/10.1038/ncomms3999

de la Vega, E., Chalk, T. B., Wilson, P. A., Bysani, R. P., & Foster, G. L. (2020). Atmospheric CO_2 during the mid-Piacenzian warm period and the M2 glaciation. *Scientific Reports*, *10*(1), 11002. https://doi.org/10.1038/s41598-020-67154-8

Dumitru, O. A., Austermann, J., Polyak, V. J., Fornós, J. J., Asmerom, Y., Ginés, J., et al. (2019). Constraints on global mean sea level during Pliocene warmth. *Nature*, *574*(7777), 233–236. https://doi.org/10.1038/s41586-019-1543-2

Dyez, K. A., Hönisch, B., & Schmidt, G. A. (2018). Early Pleistocene obliquity-scale pCO_2 variability at ∼1.5 million years ago. *Paleoceanography and Paleoclimatology*, *33*(11), 1270–1291. https://doi.org/10.1029/2018PA003349

Emiliani, C. (1955). Pleistocene temperatures. *The Journal of Geology*, *63*(6), 539–578. https://doi.org/10.1086/626295

Golledge, N. R., Levy, R. H., Meyers, S. R., Weber, M. E., Clark, P. U., Burns, J., et al. (2026). State dependent ice-sheet resonance under Cenozoic and future climates. *Communications Earth & Environment*, *7*(1), 114. https://doi.org/10.1038/s43247-025-03135-x

Guillermic, M., Misra, S., Eagle, R., & Tripati, A. (2022). Atmospheric CO_2 estimates for the Miocene to Pleistocene based on foraminiferal $\delta^{11}B$ at ocean drilling program sites 806 and 807 in the Western equatorial Pacific. *Climate of the Past*, *18*(2), 183–207. https://doi.org/10.5194/cp-18-183-2022

Hansen, J., Sato, M., Kharecha, P., Beerling, D., Berner, R., Masson-Delmotte, V., et al. (2008). Target atmospheric CO_2: Where should humanity aim? *The Open Atmospheric Science Journal*, *2*(1), 217–231. https://doi.org/10.2174/1874282300802010217

Hansen, J., Sato, M., Ruedy, R., Nazarenko, L., Lacis, A., Schmidt, G. A., et al. (2005). Efficacy of climate forcings. *Journal of Geophysical Research*, *110*(D18), D18104. https://doi.org/10.1029/2005JD005776

Hansen, J., Sato, M., Russell, G., & Kharecha, P. (2013). Climate sensitivity, sea level and atmospheric carbon dioxide. *Philosophical Transactions of the Royal Society A: Mathematical, Physical & Engineering Sciences*, *371*(2001), 20120294. https://doi.org/10.1098/rsta.2012.0294

Hieronymus, M. (2019). An update on the thermosteric sea level rise commitment to global warming. *Environmental Research Letters*, *14*(5), 054018. https://doi.org/10.1088/1748-9326/ab1c31

Hönisch, B., Hemming, N. G., Archer, D., Siddall, M., & McManus, J. F. (2009). Atmospheric carbon dioxide concentration across the mid-Pleistocene transition. *Science*, *324*(5934), 1551–1554. https://doi.org/10.1126/science.1171477

Huybers, P. (2006). Early Pleistocene glacial cycles and the integrated summer insolation forcing. *Science*, *313*(5786), 508–511. https://doi.org/10.1126/science.1125249

Köhler, P. (2023). Atmospheric CO_2 concentration based on boron isotopes versus simulations of the global carbon cycle during the Plio-Pleistocene. *Paleoceanography and Paleoclimatology*, *38*(2), e2022PA004439. https://doi.org/10.1029/2022PA004439

Köhler, P., Bintanja, R., Fischer, H., Joos, F., Knutti, R., Lohmann, G., & Masson-Delmotte, V. (2010). What caused Earth's temperature variations during the last 800,000 years? Data-based evidences on radiative forcing and constraints on climate sensitivity. *Quaternary Science Reviews*, *29*(1–2), 129–145. https://doi.org/10.1016/j.quascirev.2009.09.026

Köhler, P., & Clark, P. U. (2026). Simulating atmospheric CO_2 concentration for the Plio-Pleistocene using a new set of temperature and sea level reconstruction [Dataset]. *Pangaea*. https://doi.org/10.1594/PANGAEA.988155

Köhler, P., de Boer, B., von der Heydt, A. S., Stap, L. S., & van de Wal, R. S. W. (2015). On the state dependency of equilibrium climate sensitivity during the last 5 million years. *Climate of the Past*, *11*(12), 1801–1823. https://doi.org/10.5194/cp-11-1801-2015

Köhler, P., & Munhoven, G. (2020). Late Pleistocene carbon cycle revisited by considering solid Earth processes. *Paleoceanography and Paleoclimatology*, *35*(12), e2020PA004020. https://doi.org/10.1029/2020PA004020

Köhler, P., Stap, L. S., von der Heydt, A. S., de Boer, B., van de Wal, R. S. W., & Bloch-Johnson, J. (2017). A state-dependent quantification of climate sensitivity based on paleo data of the last 2.1 million years. *Paleoceanography*, *32*(11), 1102–1114. https://doi.org/10.1002/2017PA003190

Köhler, P., & van de Wal, R. S. W. (2020). Interglacials of the Quaternary defined by northern hemispheric land ice distribution outside of Greenland. *Nature Communications*, *11*(1), 5124. https://doi.org/10.1038/s41467-020-18897-5

Lisiecki, L. E., & Raymo, M. E. (2005). A Pliocene-Pleistocene stack of 57 globally distributed benthic $\delta^{18}O$ records. *Paleoceanography*, *20*(1), PA1003. https://doi.org/10.1029/2004PA001071

Martínez-Botí, M. A., Foster, G. L., Chalk, T. B., Rohling, E. J., Sexton, P. F., Lunt, D. J., et al. (2015). Plio-Pleistocene climate sensitivity evaluated using high-resolution CO_2 records. *Nature*, *518*(7537), 49–54. https://doi.org/10.1038/nature14145

Meckler, A. N., Sexton, P. F., Piasecki, A. M., Leutert, T. J., Marquardt, J., Ziegler, M., et al. (2022). Cenozoic evolution of deep ocean temperature from clumped isotope thermometry. *Science*, *377*(6601), 86–90. https://doi.org/10.1126/science.abk0604

Miller, K. G., Schmelz, W. J., Browning, J. V., Rosenthal, Y., Hess, A. V., Kopp, R. E., & Wright, J. D. (2024). Global mean and relative sea-level changes over the past 66 Myr: Implications for early Eocene ice sheets. *Earth Science, Systems and Society*, *4*(1), 10091. https://doi.org/10.3389/esss.2023.10091

Myhre, G., Highwood, E. J., Shine, K. P., & Stordal, F. (1998). New estimates of radiative forcing due to well mixed greenhouse gases. *Geophysical Research Letters*, *25*(14), 2715–2718. https://doi.org/10.1029/98GL01908

PALAEOSENS-Project Members. (2012). Making sense of palaeoclimate sensitivity. *Nature*, *491*(7426), 683–691. https://doi.org/10.1038/nature11574

Raymo, M. E. (1994). The initiation of northern hemisphere glaciation. *Annual Review of Earth and Planetary Sciences*, *22*(1), 353–383. https://doi.org/10.1146/annurev.ea.22.050194.002033

Raymo, M. E., Kozdon, R., Evans, D., Lisiecki, L., & Ford, H. L. (2018). The accuracy of mid-Pliocene $\delta^{18}O$-based ice volume and sea level reconstructions. *Earth-Science Reviews*, *177*, 291–302. https://doi.org/10.1016/j.earscirev.2017.11.022

Rohling, E. J., Foster, G. L., Gernon, T. M., Grant, K. M., Heslop, D., Hibbert, F. D., et al. (2022). Comparison and synthesis of sea-level and deep-sea temperature variations over the past 40 million years. *Reviews of Geophysics*, *60*(4), e2022RG000775. https://doi.org/10.1029/2022RG000775

Rohling, E. J., Gernon, T. M., Heslop, D., Reichart, G. J., Roberts, A. P., & Yu, J. (2024). Reconciling the apparent discrepancy between Cenozoic deep-sea temperatures from proxies and from benthic oxygen isotope deconvolution. *Paleoceanography and Paleoclimatology*, *39*(11), e2024PA004872. https://doi.org/10.1029/2024PA004872

Seki, O., Foster, G. L., Schmidt, D. N., Mackensen, A., Kawamura, K., & Pancost, R. D. (2010). Alkenone and boron-based Pliocene pCO_2 records. *Earth and Planetary Science Letters*, *292*(1–2), 201–211. https://doi.org/10.1016/j.epsl.2010.01.037

Shakun, J. D., Raymo, M. E., & Lea, D. W. (2016). An early Pleistocene Mg/Ca-$\delta^{18}O$ record from the Gulf of Mexico: Evaluating ice sheet size and pacing in the 41-kyr world. *Paleoceanography*, *31*(7), 1011–1027. https://doi.org/10.1002/2016PA002956

Sherwood, S., Webb, M. J., Annan, J. D., Armour, K. C., Forster, P. M., Hargreaves, J. C., et al. (2020). An assessment of Earth's climate sensitivity using multiple lines of evidence. *Reviews of Geophysics*, *58*(4), e2019RG000678. https://doi.org/10.1029/2019RG000678

Stap, L. B., Köhler, P., & Lohmann, G. (2019). Including the efficacy of land ice changes in deriving climate sensitivity from paleodata. *Earth System Dynamics*, *10*(2), 333–345. https://doi.org/10.5194/esd-10-333-2019

Tierney, J. E., King, J., Osman, M. B., Abell, J. T., Burls, N. J., Erfani, E., et al. (2025). Pliocene warmth and patterns of climate change inferred from paleoclimate data assimilation. *AGU Advances*, *6*(1), e2024AV001356. https://doi.org/10.1029/2024AV001356

Tierney, J. E., Zhu, J., King, J., Malevich, S. B., Hakim, G. J., & Poulsen, C. J. (2020). Glacial cooling and climate sensitivity revisited. *Nature*, *584*(7822), 569–573. https://doi.org/10.1038/s41586-020-2617-x

Tzedakis, P. C., Crucifix, M., Mitsui, T., & Wolff, E. W. (2017). A simple rule to determine which insolation cycles lead to interglacials. *Nature*, *542*(7642), 427–432. https://doi.org/10.1038/nature21364

Westerhold, T., Marwan, N., Drury, A. J., Liebrand, D., Agnini, C., Anagnostou, E., et al. (2020). An astronomically dated record of Earth's climate and its predictability over the last 66 million years. *Science*, *369*(6509), 1383–1387. https://doi.org/10.1126/science.aba6853

Willeit, M., Ganopolski, A., Calov, R., & Brovkin, V. (2019). Mid-Pleistocene transition in glacial cycles explained by declining CO_2 and regolith removal. *Science Advances*, *5*(4), eaav7337. https://doi.org/10.1126/sciadv.aav7337

Yamamoto, M., Clemens, S. C., Seki, O., Tsuchiya, Y., Huang, Y., O'ishi, R., & Abe-Ouchi, A. (2022). Increased interglacial atmospheric CO_2 levels followed the mid-Pleistocene transition. *Nature Geoscience*, *15*(4), 307–313. https://doi.org/10.1038/s41561-022-00918-1

Yan, Y., Bender, M. L., Brook, E. J., Clifford, H. M., Kemeny, P. C., Kurbatov, A. V., et al. (2019). Two-million-year-old snapshots of atmospheric gases from Antarctic ice. *Nature*, *574*(7780), 663–666. https://doi.org/10.1038/s41586-019-1692-3

Zhou, C., Wang, M., Zelinka, M. D., Liu, Y., Dong, Y., & Armour, K. C. (2023). Explaining forcing efficacy with pattern effect and state dependence. *Geophysical Research Letters*, *50*(3), e2022GL101700. https://doi.org/10.1029/2022GL101700

Zhu, J., & Poulsen, C. J. (2021). Last Glacial Maximum (LGM) climate forcing and ocean dynamical feedback and their implications for estimating climate sensitivity. *Climate of the Past*, *17*(1), 253–267. https://doi.org/10.5194/cp-17-253-2021

Supporting Information for

Constraints on past CO_2 and climate sensitivity from global temperature and sea level reconstructions across the Plio-Pleistocene

Peter Köhler[1], **Peter U. Clark**[2,3]

[1]Alfred-Wegener-Institut Helmholtz-Zentrum für Polar-und Meeresforschung (AWI), P.O. Box 12 01 61, 27515 Bremerhaven, Germany

[2]College of Earth, Ocean, and Atmospheric Sciences, Oregon State University, Corvallis, OR 97331, USA

[3]School of Geography and Environmental Sciences, University of Ulster, Coleraine, BT52 1SA, Northern Ireland, UK

Content

All references mentioned in the SI are contained in the reference list of the main text.

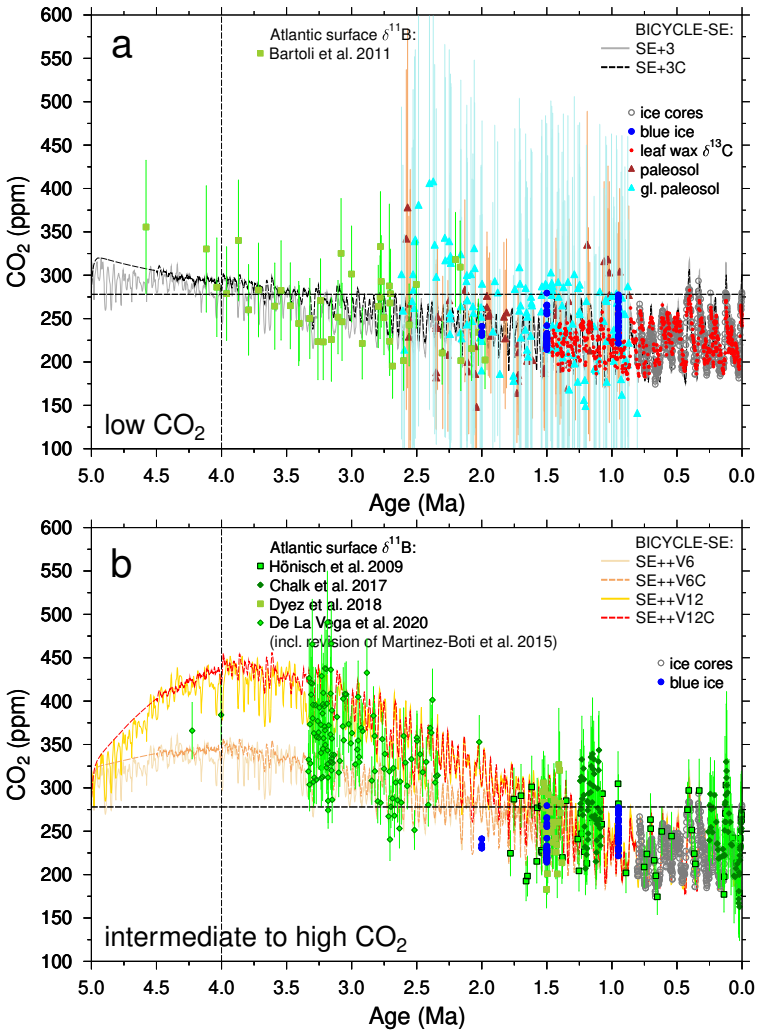

Figure S1. Atmospheric CO_2. Realisations with either (a) low or (b) intermediate to high CO_2 in the Pliocene/Early Pleistocene. Simulations results of scenarios SE+3, SE++V6 and SE++V12 from BICYCLE-SE as already published (Köhler, 2023) or (with the extension C in the scenario names) when based on the new temperature and GMSL reconstructions (this study). Scenarios SE+3(C) contain no long-term trend in volcanic outgassing of CO_2, and a weak CO_2-dependency of the weathering fluxes, while in scenarios SE++V6(C) and SE++V12(C) a strong CO_2-dependency of continental weathering is assumed and CO_2 ougassing from volcanism decreases linearly over time between 4.5 and 1.0 Ma by either 6 or 12%, respectively. Vertical lines at 4 Ma marks the end of the period affected by model spin-up in the simulation results. CO_2 data based on ice cores (Bereiter et al., 2015), blue ice (Yan et al., 2019), paleosol (Da et al., 2019), paleosol from glacial (gl.) periods only (Da et al., 2025), leaf wax δ^{13}C (Yamamoto et al., 2022) and δ^{11}B from Atlantic cores as compiled in Dyez et al. (2018) with updates from de la Vega et al. (2020), but marked as initially published (Hönisch et al., 2009; Bartoli et al., 2011; Chalk et al., 2017; Martínez-Botí et al., 2015).

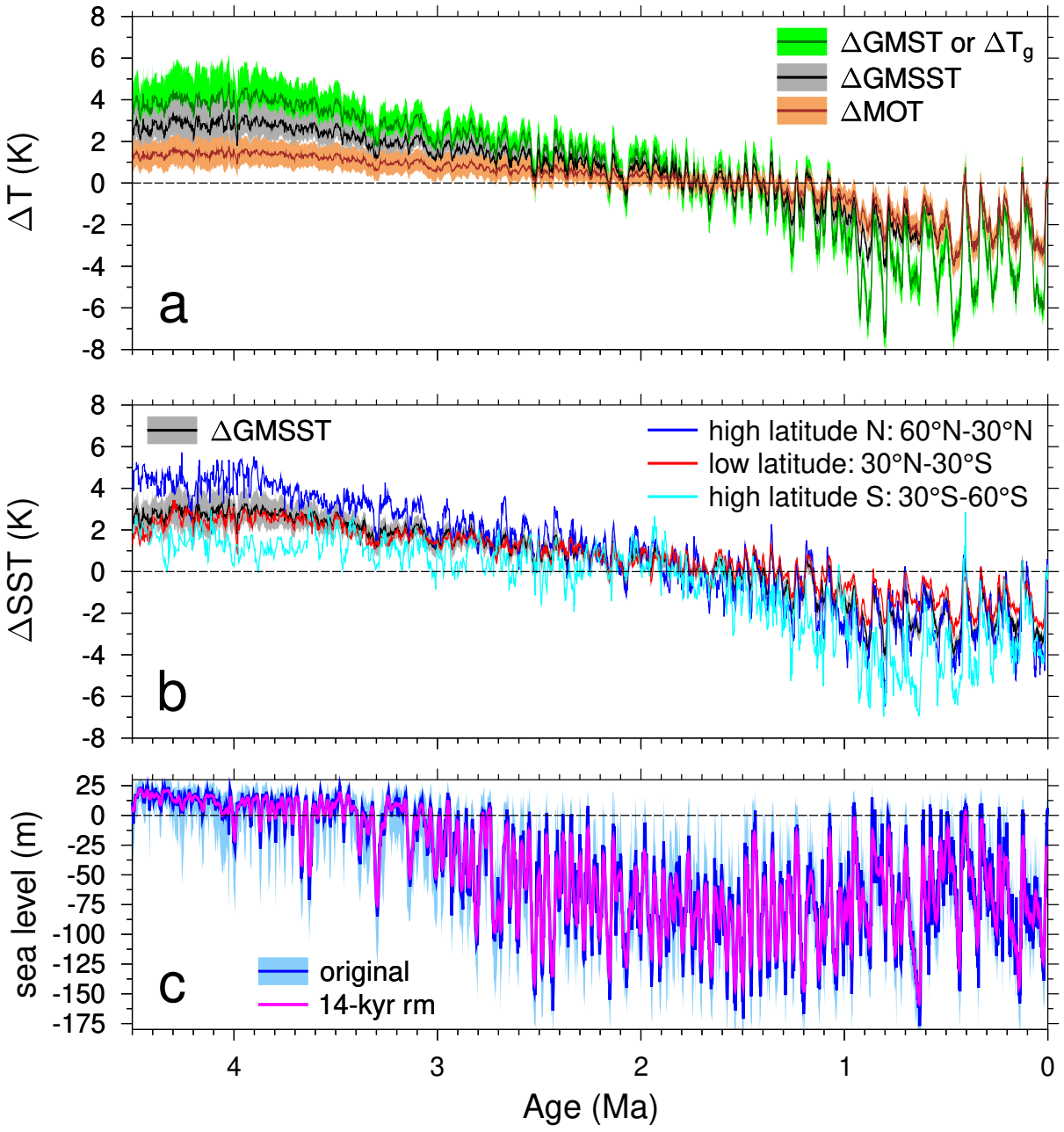

Figure S2. The new set of reconstructed climate changes (CL1, CL2, CL3). (a) Global mean surface temperature (GMST or ΔT_g), global mea sea surface temperature (GMSST), mean ocean temperature (MOT); (b) latitudinal changes in sea surface temperature (SST) compared to GMSST; (c) global mean sea level, originally, and as 14-kyr running mean (rm), which due to changing rates that agree better with independent estimates is used to force the model. Plotted shadings represent 1σ uncertainities.

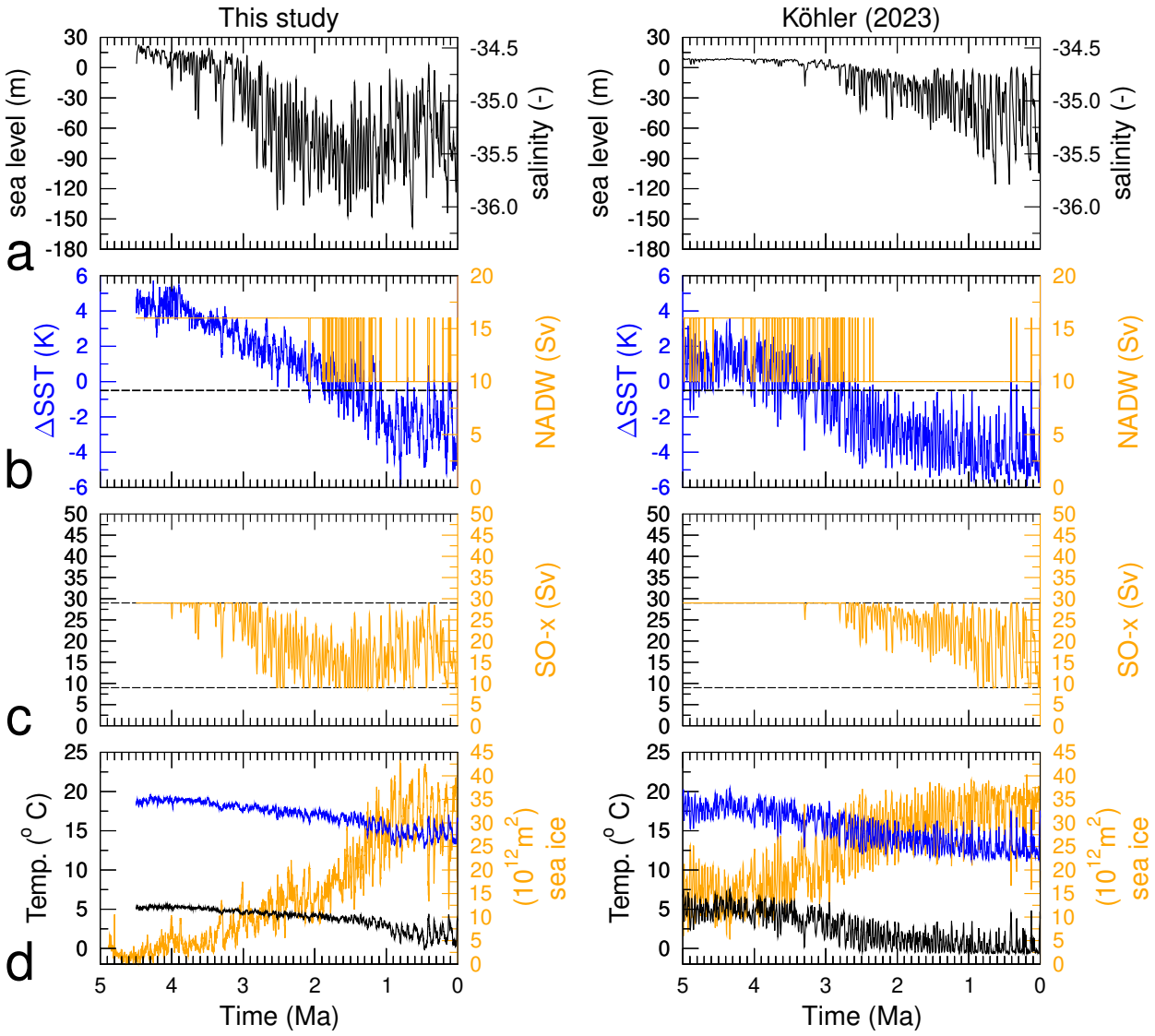

Figure S3. Differences in the time-dependent forcing of the BICYCLE-SE model as used here from its previous application. Left: this study; right: as used in Köhler (2023). (a) Sea level resulting in the corresponding mean ocean salinity (right y-axis). (b) North Atlantic Deep Water (NADW) formation (orange, right y-axis), is either in interglacial or glacial mode, following the applied SST forcing (blue, left y-axis) in the high-latitude Atlantic, horizontal line marks the SST threshold for switching between both states. (c) Southern Ocean vertical mixing (SO-x: surface-to-deep ocean flux) is calculated as function of sea level with upper and lower limitation (9–29 Sv) marked by horizontal lines. Alternative dependencies of SO-x as function of Southern Ocean SST have also been used before (Köhler, 2023), but are not followed here any further. (d) Mean ocean temperatures (black) and global mean SST (blue) averaged within the model. Right y-axis: global integrated sea ice area (orange).

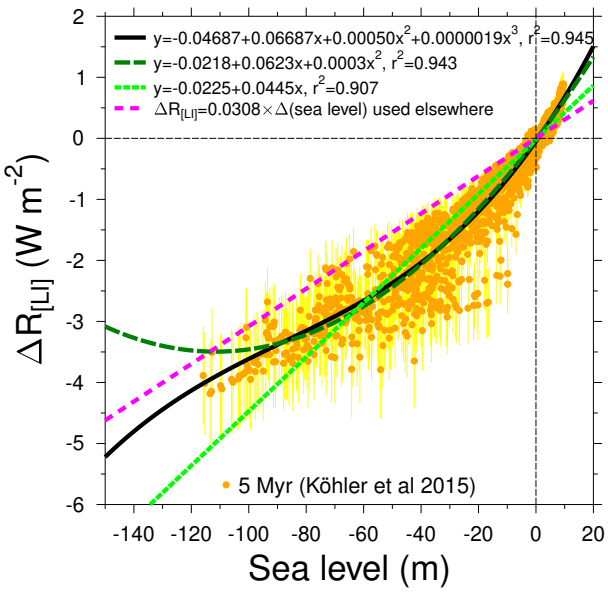

Figure S4. Relation of land ice-albedo forcing ($\Delta R_{[\mathrm{LI}]}$) and sea level, revised from Köhler et al. (2015). Scatter plot of sea level change (de Boer et al., 2014) against land ice albedo forcing $\Delta R_{[\mathrm{LI}]}$ (Köhler et al., 2015) based on the 3-D ice-sheet model ANICE. Data are approximated with fits of different order. The third order non-linear fit gives the best results and is applied here. For comparison a fit based on sea level change as applied in other applications (Hansen et al., 2008; Martínez-Botí et al., 2015) is shown as dashed line.

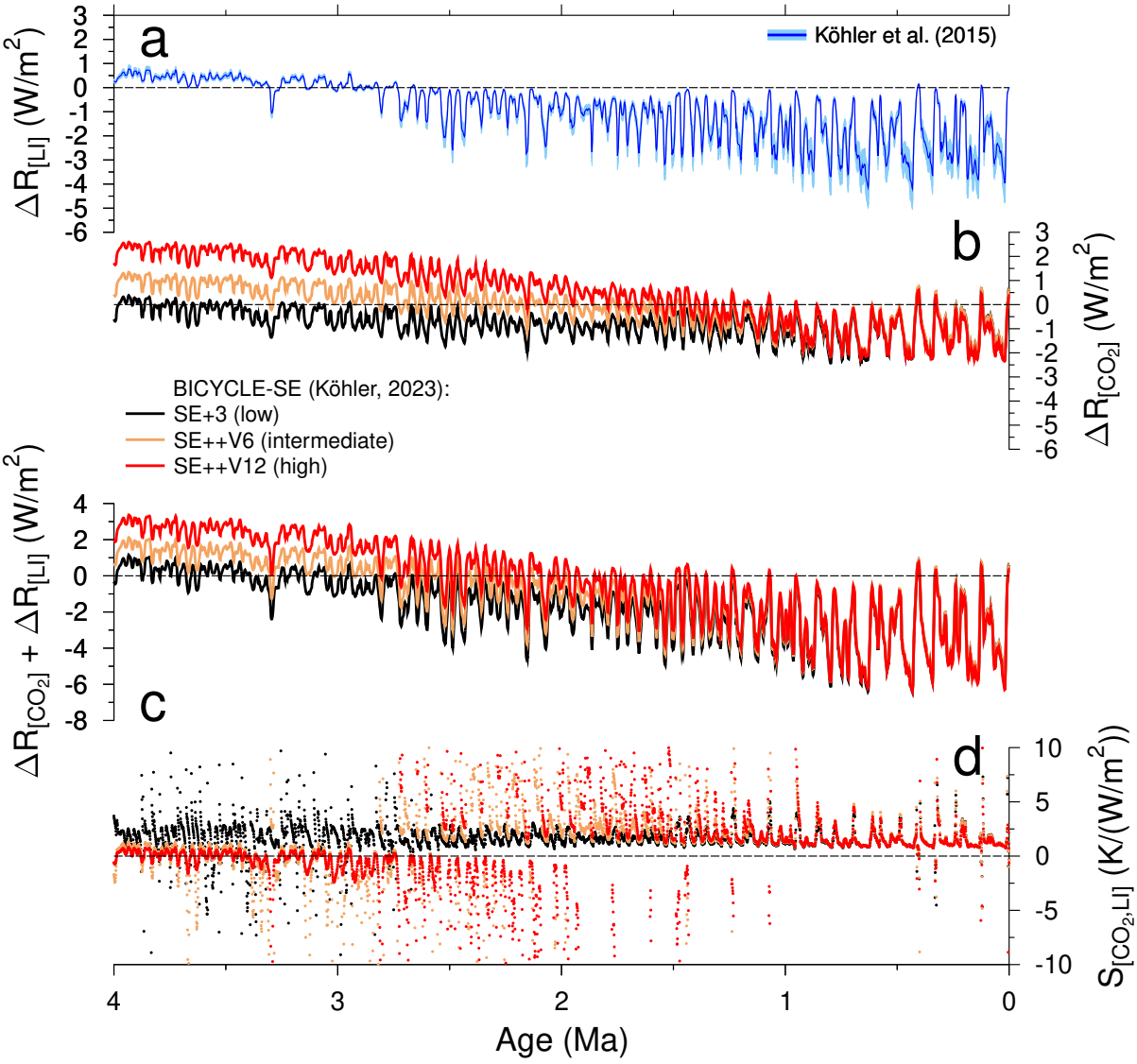

Figure S5. Radiative forcing of the **previous approach** (Köhler et al., 2015; Köhler, 2023). (a): Land ice albedo radiative forcing ($\Delta R_{[LI]}$) is based on a land ice model. (b) Radiative forcing of CO_2 ($\Delta R_{[CO_2]}$) based on the noted simulations scenarios using BICYCLE-SE. (c) Summed up forcing of $\Delta R_{[CO_2]} + \Delta R_{[LI]}$. (d) Pointwise specific climate sensitivity $S_{[CO_2,LI]}$ following Equation 1. Colorcode in (b) is also applied in (c,d).

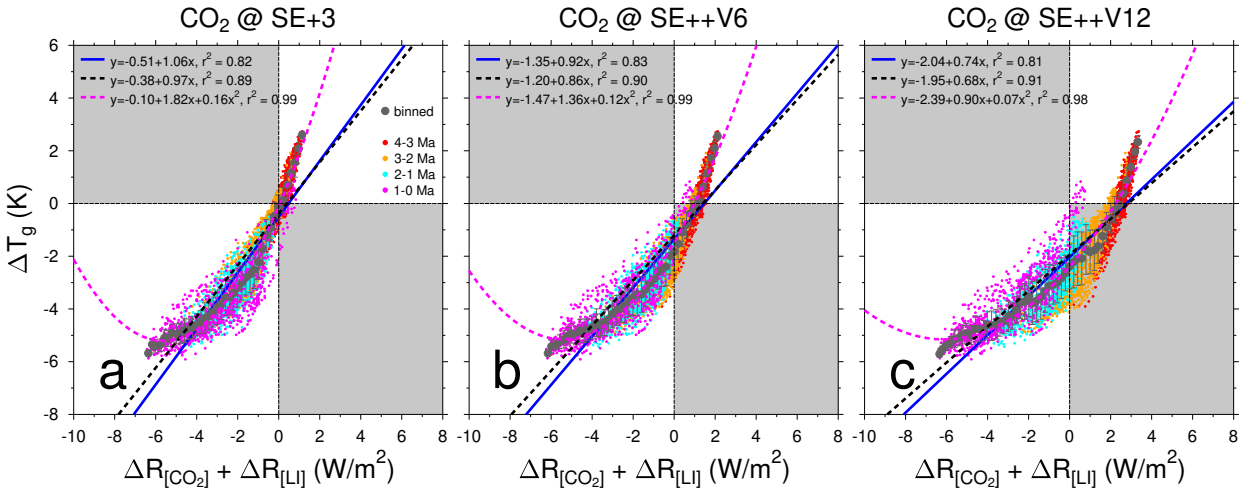

Figure S6. Scatterplots of ΔT_g versus radiative forcing ($\Delta R_{[CO_2]} + \Delta R_{[LI]}$) based of data of the past 4 Ma from the **previous approach** (Köhler et al., 2015; Köhler, 2023). The applied CO_2 in different subpanels is taken from the simulation scenario mentioned in the headings. Original data (one point each 1 kyr, colorcoded by time, see legend in (a)) are averaged in bins in ΔR of 0.2 W/m^2 width (dark grey circles with $\pm 1\sigma$). Regressions are either using the original (blue lines) or the binned (black broken lines, magenta broken lines for the second order polynomial) data. Grey shaded areas are those in which ΔT_g and ΔR have the opposite sign. Variables in these areas might be possible due to various feedbacks, but more naturally data should preferably fall in the white quadrants.